



RF and Electronics Design of the Compact Ocean Wind Vector Radiometer

Frank Maiwald , Oliver Montes, Sharmila Padmanabhan , Amy Wu , Zachary Pannell, Violet Torossian , Alireza Bakhshi, Damon Russell, Jordan Tanabe, Hamid Javadi, Chris Holman, Maurice Aghion, Richard Redick, Amarit Kitiyakara , and Shannon Brown

Abstract—The Compact Ocean Wind Vector Radiometer (COWVR) was developed at the Jet Propulsion Laboratory as a proof of concept technology demonstration mission for the Air Force. COWVR is a fully polarimetric imaging radiometer system operating at 18.7, 23.8, and 33.9 GHz. Its receiver subsystem is based on the Jason-3 advanced microwave radiometer, which was launched in early 2016 and is currently in operation. Its enabling components are presented in this article, including the phase-matched waveguide components, noise injection, receivers, and polarimetric backend units.

Index Terms—Polarimetric microwave radiometer, noise sources, phase-matched RF components.

I. INTRODUCTION

COWVR'S RF subsystem consists of the Jason-3 advanced microwave radiometer (AMR) design. Its fully polarimetric radiometer channels are intended to retrieve the ocean surface wind vector, as well as other key environmental parameters such as precipitable water vapor, cloud liquid water, precipitation rate, and sea ice. The measurement of ocean surface vector winds by a polarimetric microwave radiometer was first demonstrated by the Naval Research Laboratory WindSat radiometer, which was launched in 2003 [1]. As this was a first-of-its-kind measurement, the system was developed from conventional technology to ensure successful demonstration of the new measurement technique [2] and consequently had to employ a large mass and power (450 kg and 350 W). Compared to WindSat, the COWVR

Manuscript received May 9, 2020; accepted June 22, 2020. Date of publication June 25, 2020; date of current version July 8, 2020. This work was supported by the Jet Propulsion Laboratory, California Institute of Technology, and funded by the U.S. Air Force. (Corresponding author: Frank Maiwald.)

Frank Maiwald, Oliver Montes, Sharmila Padmanabhan, Amy Wu, Violet Torossian, Damon Russell, Jordan Tanabe, Hamid Javadi, Richard Redick, Amarit Kitiyakara, and Shannon Brown are with Jet Propulsion Laboratory, California Institute of Technology, Pasadena, CA 91109 USA (e-mail: frank.maiwald@jpl.nasa.gov; oliver.montes@jpl.nasa.gov; sharmila.padmanabhan@jpl.nasa.gov; amy.wu@jpl.nasa.gov; violet.torossian@jpl.nasa.gov; damon.russell@jpl.nasa.gov; jordan.tanabe@jpl.nasa.gov; hamid.javadi@jpl.nasa.gov; richard.redick@jpl.nasa.gov; amarit.kitiyakara@jpl.nasa.gov; shannon.brown@jpl.nasa.gov).

Zachary Pannell is with Lockheed Martin, Denver, CO 80221 USA (e-mail: zpannell@gmail.com).

Alireza Bakhshi is with Jet Propulsion Laboratory, California Institute of Technology, Pasadena, CA 91109 USA, and also with B&A Engineering, Inc., Costa Mesa, CA 92626 USA (e-mail: Alireza.Bakhshi@jpl.nasa.gov).

Chris Holman and Maurice Aghion are with Microwave Engineering Corporation, North Andover, MA 01845 USA (e-mail: c_holman@microwaveeng.com; m_ghion@microwaveeng.com).

Digital Object Identifier 10.1109/JSTARS.2020.3005041

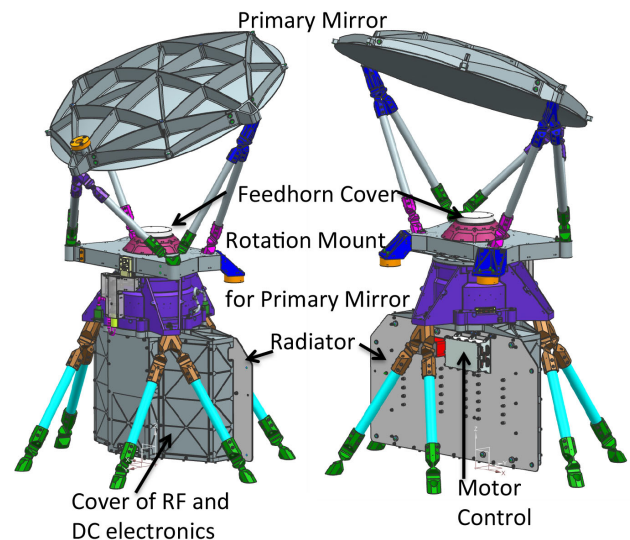


Fig. 1. COWVR instrument model, 1.5 m high, the base is approx. 1×1 m. The only moving components are the main reflector and the rotation mount. The RF, digital, and power electronics are thermally isolated from the spacecraft via bipods and has its own radiator.

system uses a novel data retrieval concept to reduce the system complexity, which in turn significantly reduces its cost, mass (60 kg), power (60 W), and volume while seeking to maintain the same level of wind vector retrieval accuracy.

II. SYSTEM DESCRIPTION

The RF and dc electronic assemblies are bolted to a radiator that is situated underneath the rotation mount and the primary reflector, see Fig. 1. The primary reflector has a diameter of approximately 0.75 m and rotates at 30 RPM around a fixed FeedHorn Assembly (FHA) positioned at the beam center. No electrical connections are made between the movable part and the rest of the instrument, which minimizes complexity. Due to its rotation, the primary mirror has been designed to receive a projected conical beam from Earth's surface. This signal can be decomposed during data analyses at the ground stations to draw polarimetric spatial maps of Earth's surface.

With the primary reflector, the signal is funneled into the FHA and then sends to the OrthoMode-Transducer (OMT), which splits the incoming signal into H and V that have orthogonal

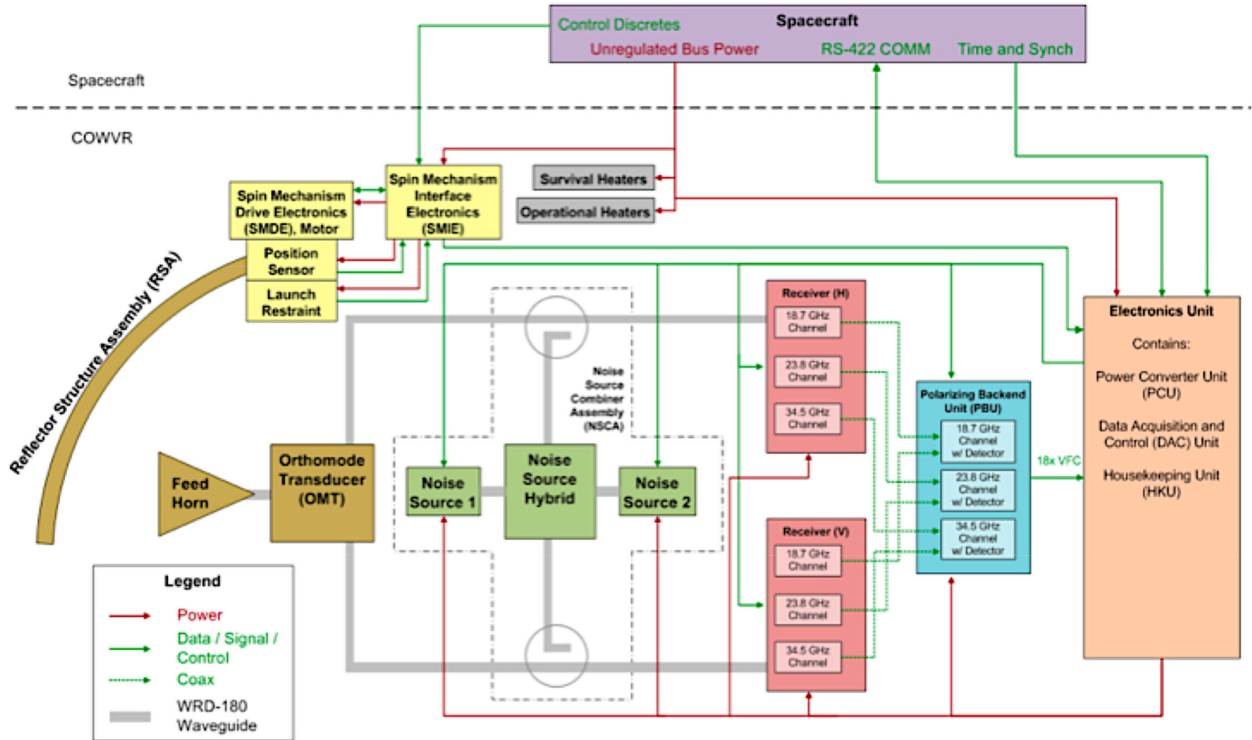


Fig. 2. Block diagram of the COWVR instrument. The signal is focused into the FHA then transferred to the OMT. A calibrated noise signal is injected by the NSH with its two noise sources, amplified by receivers, routed to the PBUs, and finally processed in the EU.

polarization. Both polarized signals are amplified by a modified Jason-3 receiver [3] with radiometers at 18.7, 23.8, and 33.9 GHz and then recombined in polarimetric backend units (PBUs) for each frequency channel, see Fig. 2. The three PBUs split the H and V signals into six Stokes parameters. These analog signals are transformed by voltage-to-frequency converters (VFC) into pulse trains. All pulses are counted with a field programmable gate array (FPGA) in the electronics unit (EU). The EU controls two receivers, reads out three PBUs, and controls two noise sources. It also supplies all bias voltages and provides housekeeping for temperature sensing. The sensors are placed at temperature-sensitive components to support the calibration of the RF subsystem.

The RF subsystem is calibrated with an external Noise Source Calibration Assembly (NSCA) (see Fig. 3). This subassembly has two noise sources (NS1/2, same design as used previously [3]) and two couplers to feed into the H and V waveguides of the instrument. In the instrument configuration, both NS signals (see Fig. 2) are injected into the Noise Source Hybrid (NSH), which is capable of generating known correlated polarized signals by injecting correlated noise with a defined phase offset between the two receiver chains. During the build, the entire signal train needed to have well-matched phase and amplitude from the FHA down to PBUs. Any deviations would have resulted in a systematic bias in the Stokes parameters, which could have been challenging to remove during data post-processing or tuning of RF hardware.

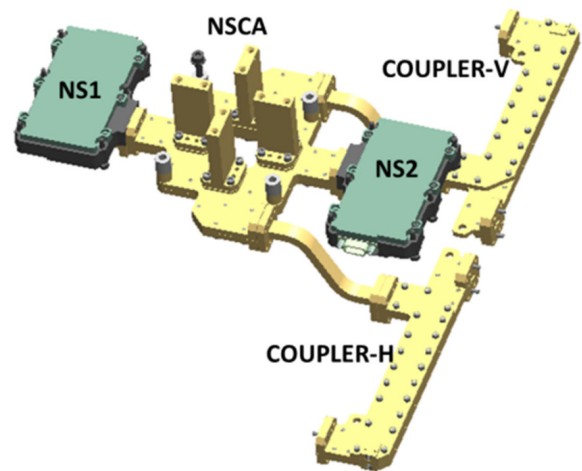


Fig. 3. Assembly of the NSCA, noise sources NS1/NS2, and H/V directional couplers.

A. Waveguide Components in the Front-End

The waveguide components at the front-end are comprised of the FHA, OMT, waveguides, and directional couplers (see Fig. 4). The FHA had been developed for the AMR on Jason-3, and its design was inherited from Jason-3. Meanwhile, the OMT was redesigned by Microwave Engineering Corporation (MEC) to meet the tight phase and amplitude requirements. The FHA

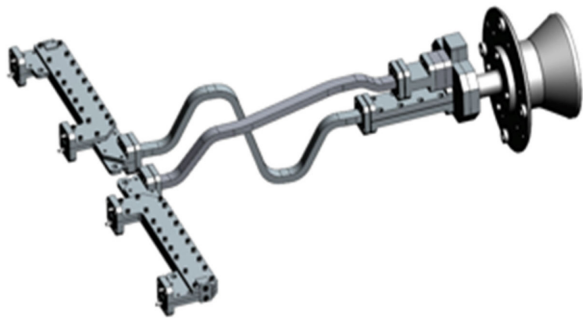


Fig. 4. Waveguide components of COWVR: V/H-coupler, V/H-WRD-180, OMT, FHA.

TABLE I
OMT CHARACTERISTIC RF PERFORMANCE

	Requirement	Measured
Insertion Loss [dB]	< 1.2	1.1
Phase slope balance [deg/MHz]	<0.03	0.018
H/V isolation [dB]	>35	51

guides signals from the primary reflector into the RF subsystem. The OMT later splits the incoming signal into orthogonal linear polarized H and V components. MEC enhanced the OMT with a tight phase slope balance between the H and V outputs. Each internal section of the OMT design was examined in detail with HFSS, a commercially available finite element method solver for electromagnetic structures distributed by Ansys [4].

Multiple units were fabricated at the same time, and the best performing unit was reserved for the flight implementation. At the end of the instrument integration phase, a gap between the long waveguides and the couplers was eliminated by carefully bending the long waveguides. The phase matching and insertion loss were carefully tuned (*in situ* measurements with a vector network analyzer, VNA) during this bending process to ensure that requirements were met while eliminating the gap. The main requirements for the front-end are listed in Table I. The OMT performance was also verified by detailed VNA measurements using a circular waveguide section between two units. The S-parameters of all components were used in the instrument model to predict the overall performance.

B. Noise Source Calibration Assembly (NSCA)

Two noise source units were coupled into the NSCA (see Fig. 3). One side of the unit employed a 90° phase shifter, which generated a phase difference of the injected noise between the H and V, see Fig. 5. These H and V signals were then coupled with directional waveguide couplers into the two flight receivers. Though this arrangement did not provide a complete polarimetric verification, it was sufficient to estimate the polarimetric gain and offset of the receivers. The requirements for the NSCA are provided in Table II. Combining two different noise sources, NS1 and NDS2, with the implemented design of the NSCA requires a differential phase within 50° and 120° (Fig. 6 shows the simulated range). The range of the brightness temperature simulates the expected observation and is within the range of brightness temperature of the internal noise sources.

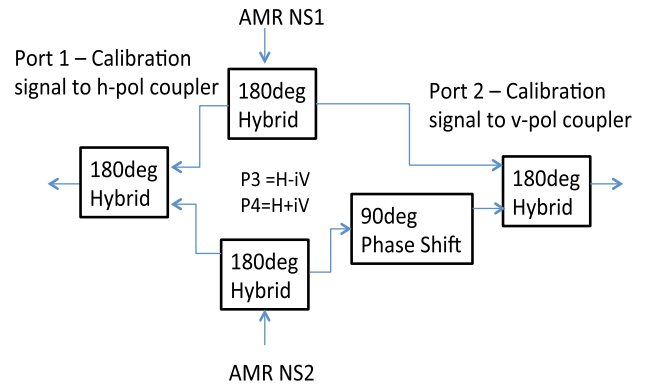


Fig. 5. NSCA was based on 180° hybrids and one 90° phase shifter, which allows injection of a known polarized signal into the H and V.

TABLE II
NSCA PERFORMANCE, REQUIREMENTS SET TO MEET THE INSTRUMENT SPECIFICATION

	Required	Measured
H/V phase difference [degree]	50 - 120	71 – 85*
Directivity [dB]	>28	30 - 35
Brightness Temperature [K]	150 - 375	158 – 355
Temperature Coef. [dB/C]	<0.01	0.02 – 0.008

Note: *simulated data which were confirmed by measurements within 2 degrees.

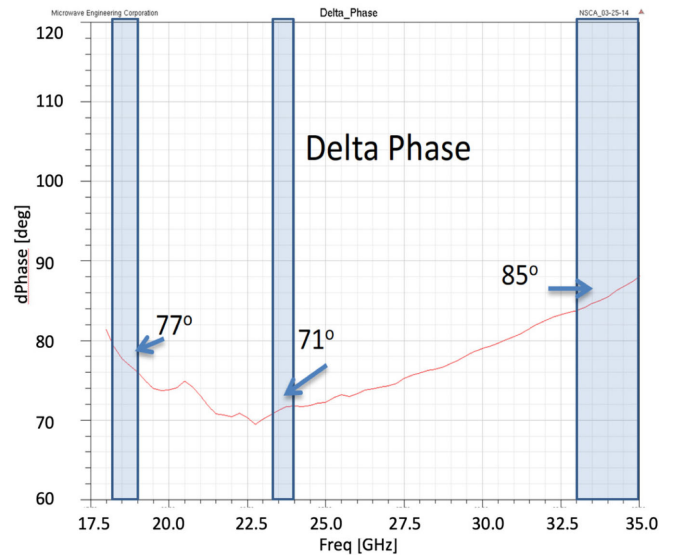


Fig. 6. HFSS simulations of the NSCA. The H/V phase difference varies from 71° to 85° over all three frequency bands.

The hardware capability drives the directivity and temperature coefficient. The changes in RF performance of the NSCA and OMT was simulated over the operating temperature range with HFSS and later confirmed by measurements. The comparison showed negligible differences between the simulations and the actual measurements. Fig. 6 shows the H/V phase difference over the three radiometer channels.

The receiver design (see Fig. 7), which was originally inherited from Jason-3 [3], required only minimal changes to the

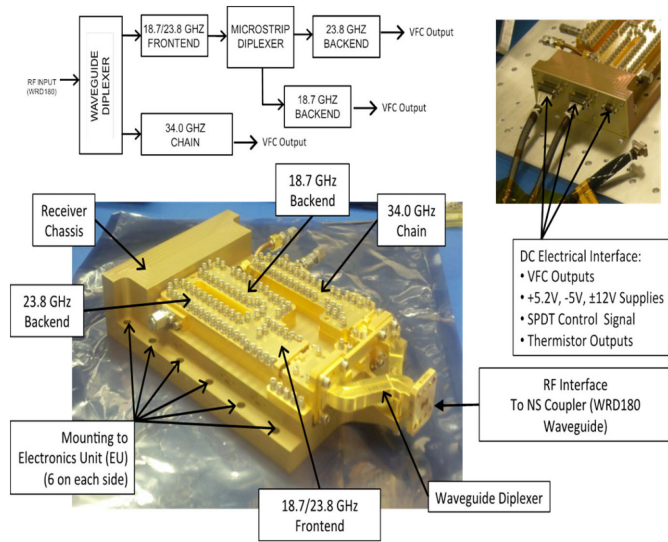


Fig. 7. Receiver assembly with three receiver channels at 18.7/23.8, and 34 GHz . The diplexer is attached to the inputs of these carriers.

readout electronics. Each receiver contains three radiometric channels at 18.7, 23.8, and 33.9 GHz as well as dc electronics to bias the LNAs and two Dicke switches. A waveguide-diplexer is connected to the input of each receiver. It separates the two frequency ranges from the WRD-180 output of the H and V waveguide couplers.

The purpose of building two identical receivers for the H and V sides was to ensure tight phase matching, same amplitudes, and matching bandpass between the receivers. This was achieved by testing each component: Dicke switch circuits, isolator, LNAs, and bandpass filters during the RF circuit assembly. VNA characterization of each stage during the flight build was also performed to meet the next level requirements. Some of the results are shown in Figs. 8 and 9.

All individually measured data were placed in an ADS (Advanced Design System from Keysight) [5] model of the RF subsystem, and the datasets were verified to meet the overall requirements. Each RF subcircuit in the receivers and the PBUs was matched. Coaxial lines and attenuators with low VSWR were selected to minimize potential mismatches. These individual optimizations during implementation yielded very low systematic biases for all three 18.7, 23.8, and 33.9 GHz PBUs after H and V signals were mixed. Each Stokes parameter of V, H, +45, -45, and right and left circular was adjusted before the final testing of the PBUs. The results showed only negligible noise and bias differences.

C. Polarimetric Backend Units

COWVR uses three PBU with H and V input signals at 18.7, 23.8, and 33.9 GHz . These hybrid backends perform the analog in-phase and quadrature-phase cross-correlation of the two signals to produce the Stokes outputs. The bandpass of each PBU was designed to be wider than the ones from the receivers to detect maximal signal strength. Each PBU includes an RF

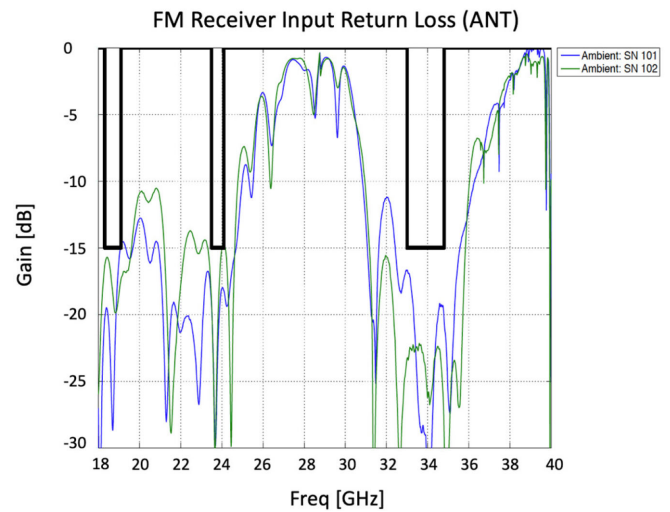
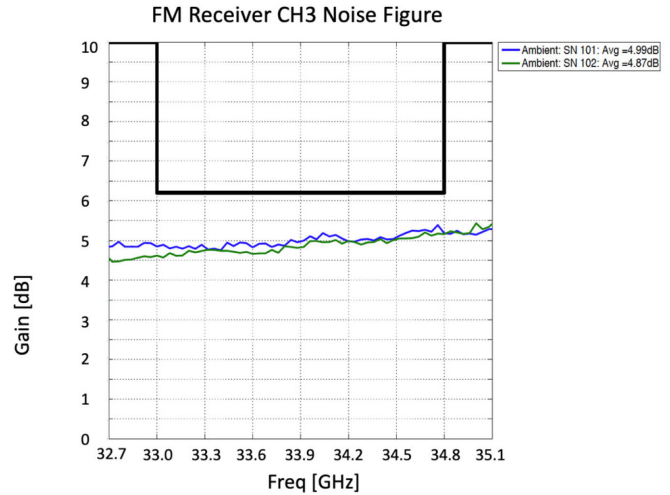


Fig. 8. Top, noise figure of CH3 (34 GHz) of both receivers. The noise figure is around 5 dB with less than 0.3 dB between the two receivers. Bottom, the input return loss matches between the two receivers very well within the three-frequency band.

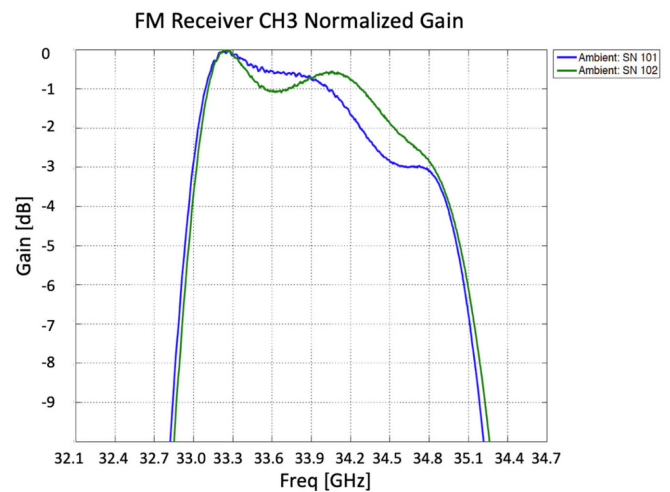


Fig. 9. Normalized gain of both receivers. The measured differences are less than 1 dB between the two receivers.

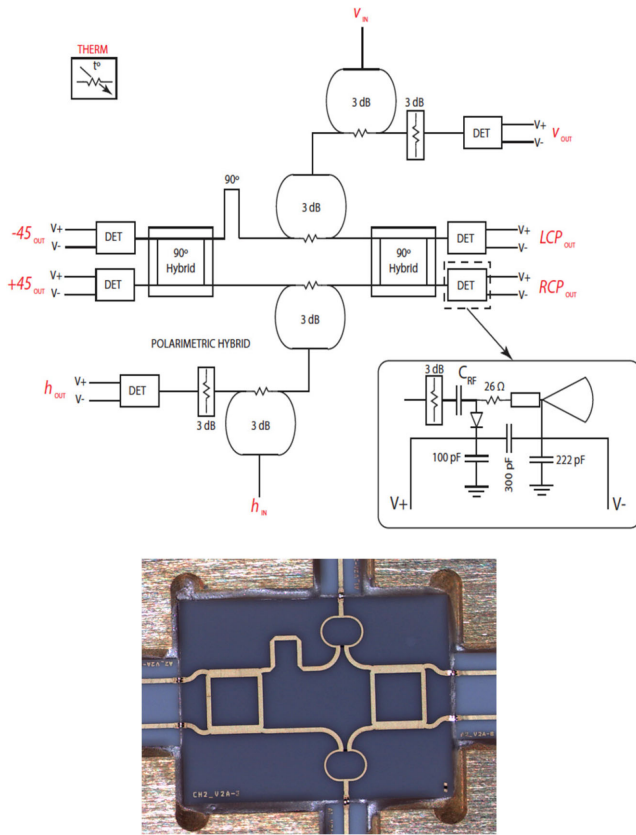


Fig. 10. RF block diagram and photo of the RFM for one PBU.

Module (RFM in Fig. 10) that extracts the Stokes components (H, V, +45, -45 and left and right circular polarized) and dc readout electronics.

The essential part of the RFM is the polarimetric hybrid to separate circular and linear polarized signals from the H and V inputs. For this, the input signals are divided in half and transmitted to H and V outputs, respectively. The signals then were split again. The first half is passed through a 90° hybrid, which generated right and left circular polarized signals. The second half of the signal is processed through a second 90° hybrid with a 90° phase shift in the V side. The resulting outputs include +45 and -45 polarized components (see Fig. 10). All six signals are detected within the linear detection range of tunnel diode detectors, then post amplified, and finally converted from analog signals to frequency trains with a VFC. The FPGA is located in the DAC assembly of the EU. It counts the pulse train of all six channels at each frequency with a 16-bit resolution.

Tuning of the post-detector amplifier gain was performed to ensure equal signal strength for small polarimetric signals. In addition, all RF components were selected to match the phase and amplitude during the subassembly phase, which allowed us to meet the performance requirements listed in Table III.

Two-phase locked Agilent synthesizers (see Fig. 11) at 5 mHz frequency offset were injected into the H and V branches of each PBU to analyze the polarimetric efficiency, channel cross-talk, and isolation leakage. As the first step, the PBUs were checked before being integrated into the entire RF subsystem.

TABLE III
PBU PERFORMANCE

	Required	Measured
Polarimetric Efficiency [%]	>90	>99
VFC Resolution [K/count]	<0.6	0.5 – 0.6
Video Bandwidth [KHz]	>20	21.5*

Note: *simulated in PSPICE.

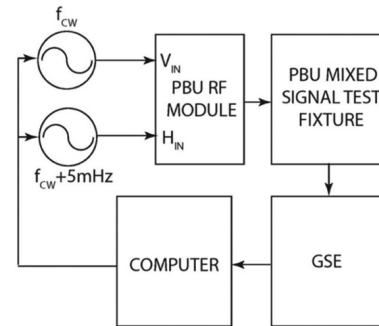


Fig. 11. Phase locked synthesizers with 5 mHz offset injected into the H and V side of the PBUs.

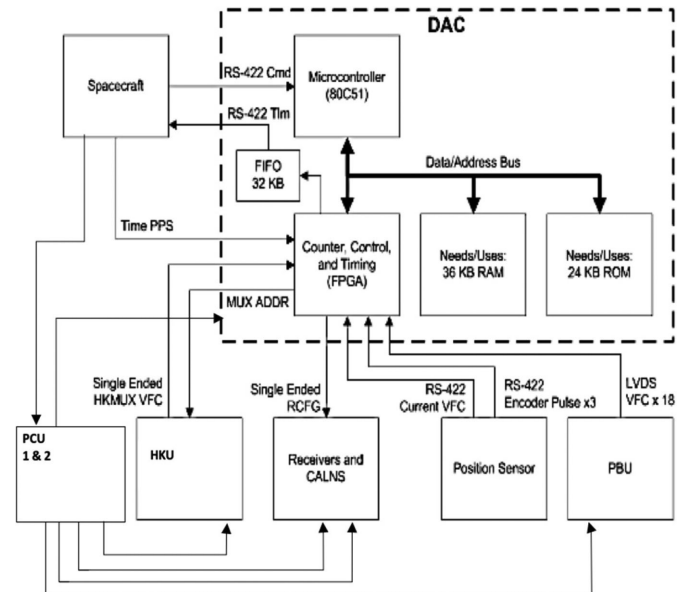


Fig. 12. Block diagram of the EU, which contains three elements PCU, HKU, and DAC each in its own chassis.

Both injected signals beat sweeping H/V phase difference over 2π every 200 s with 5 ms integration time.

D. Readout Electronics

The central part of the COWVR electronics subsystem (EU) is the readout backend (see Fig. 12). This element contains a Power Conversion Unit (PCU), which provides all bias voltages for the RF and EU subsystems. The Data Acquisition and Control Unit (DAC) interfaces with the spacecraft (S/C). Each of the receivers, noise sources, and PBUs, and a House Keeping Unit

(HKU) is packaged in a separate chassis with RF seals (Spira-Shield) on the connector plates and lids to mitigate RFI pickup. This arrangement of the connectors is designed to fit in small packages. The DAC contains an 8051 CPU with 64 Kbyte RAM and ROM as well as an Actel FPGA RTSX72SU to share a 32 Kbit FIFO (first-in-first-out memory) with the CPU. All interface drivers to the S/C are serial RS 422 interfaces. The firmware has 18 counters for the science signals from the PBUs and one counter for all temperature sensors from the HKU. It serves all control lines to the receivers and noise sources and handled the timing for the FIFO and the measurement cycle.

The operating system of the DAC has an interrupt-controlled architecture, and the firmware architecture employs a single thread with one science operational mode to keep the operation simple. By using a measurement sequence table, different science configurations can be selected. The spacecraft computer serves only as relay for the uploading command. Furthermore, uploading the entire instrument software into the memory is possible via a special command. A pointer redirects the CPU to run the code from RAM. A watchdog was hard-wired in the FPGA to prevent freezing of the system. The data and telemetry are transferred via memory mapping in a FIFO by the FPGA.

III. SYSTEM VERIFICATION

The main requirement of COWVR [6] is to measure the brightness temperature (TB) with an RMS error of less than 0.5 K with a goal of 0.3 K. This error is broken down into three main components and verified by test and analysis. (1) The frequency-dependent measurement noise specification (0.31K for 18.7 GHz, 0.33 K for 23.8 GHz, and 0.18K for 33.9 GHz) includes the pseudo-random high-frequency uncertainty in the measurement, which is due to the inherent noise in the scene measurement and additional noise that is introduced during the operational calibration process. (2) The antenna temperature calibration error allocation (0.18 K all three radiometer channels) includes the error in accounting for thermal variations in the front-end that are outside of the calibration loop. (3) The brightness temperature calibration error allocation (0.15 K all three radiometer channels) includes uncertainty in estimating the main beam brightness temperature given the antenna pattern as well as dynamic pointing errors. TB error margin is withheld at the instrument level. The electronics contributed to the measurement noise and antenna temperature error budget terms.

The measurement noise of the instrument performance was verified at each stage of the instrument build. Simulations and measurements of noise sources, receivers, OMT, waveguides, coupler, PBUs, and NSH were obtained (some of the results are provided in Section II A–D), and the measurement noise determined. The polarimetric performance of the RF subsystem was measured over the science temperature range to ensure the calibration of the instrument on-orbit. The goal was to bound the magnitude of potential calibration biases and to characterize dynamic errors that might not be mitigated by on-orbit calibration. The end-to-end measurement noise was verified during thermal vacuum testing giving 0.26 K for 18.7 GHz, 0.25 K for

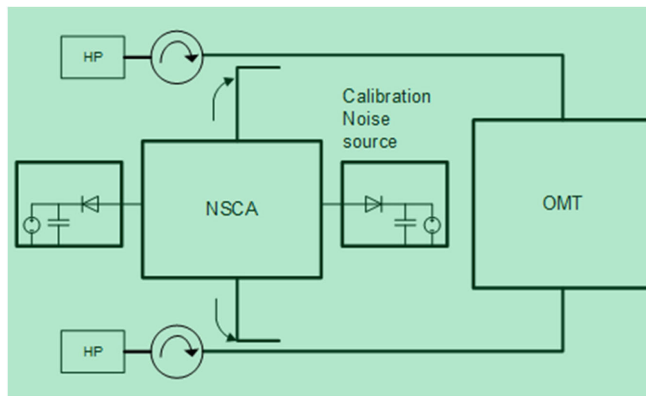


Fig. 13. Block diagram of EPCS. A copy of the noise source calibration system was implemented with external HP noise sources. The signals were coupled versus a circular waveguide section into the OMT of the flight ES of the COWVR instrument.

23.8 GHz, and 0.13 K for 33.9 GHz, which is less than the allocated error (1).

The antenna temperature calibration of the different Stokes products was carefully examined. For this purpose, two methods of injecting RF signals into the RF subsystem were employed. One was to use a temperature-stabilized correlated noise source system called External Polarimetric Calibration Source (EPCS), see Fig. 13. The EPCS included copies of OMT, two noise sources, and an NSCA. The two Jason-3 style noise sources were coupled via the NSCA into WRD-180 waveguide couplers. Two commercial noise sources were attached to the thru-ports of the couplers to inject H and V products individually. The amplitude of the generated noise signals were then calibrated relative to a with a cryogenic calibration target at ~ 80 K and room temperature termination (~ 300 K). The polarimetric output of the EPCS was determined by measuring the phase difference between the H and V ports with a network analyzer. The EPCS was held at a stable temperature outside of a thermal chamber while the COWVR radiometer subsystem was thermally cycled inside the chamber. The generated noise levels from the EPCS were found to be stable during the test by inspection of ratios of the noise sources. The EPCS enabled verification of polarimetric calibration over instrument temperature.

A second end-to-end test was conducted with the instrument at ambient temperature and pressure. For the validation test, $\lambda/4$ -waveplates (retardation plate) and polarizer grids were utilized for each of the three frequencies similar to the calibration of airborne polarimetric radiometers [7]–[11]. The polarizer grids were fabricated by using printed wire grid technology. The wire diameter and its spacing were optimized for 18.7 (at bandwidth (BW) of 750 MHz), 23.8 (BW 500 MHz), and 34 GHz (BW 1800 MHz) at 45° tilt. The waveplates were fabricated on the dielectric material Rexolite 1422 with fill-factor of 0.35, transmissivities of 99%, and reflectivities of less than 0.008% for the frequencies of interest. The spacing between grooves and their depth was optimized for 52° at the frequencies and BWs, as mentioned earlier. The test setup consisted of an aluminum box

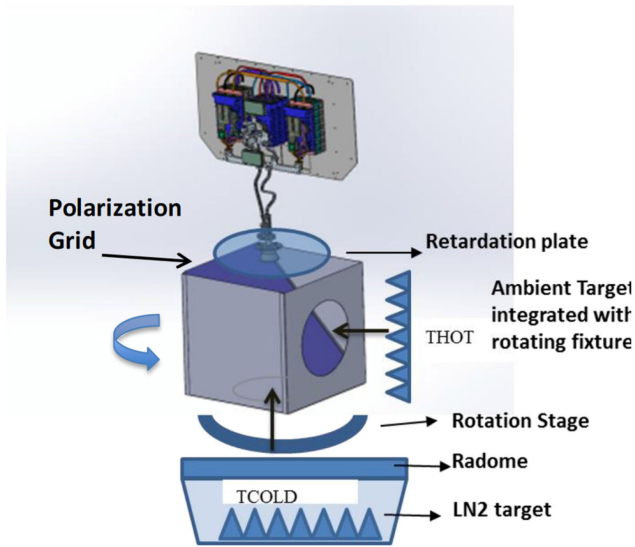


Fig. 14. Polarimetric setup to verify polarimetric performance.

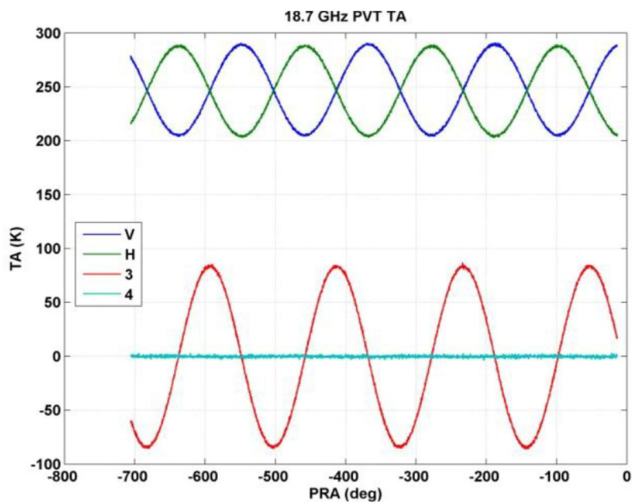


Fig. 15. On test case of the measured polarimetric performance with the polarimetric setup test setup. The 3rd Stokes parameter in red is displayed and the 4th Stokes in light blue line is flat (configuration of input signal). H in green and V in blue are in a 180° phase relation and have the same strengths.

(see Fig. 14) with an absorber inside, one window for the cold view (liquid nitrogen), and one hot target at room temperature. This box was mounted on a rotational stage for 360° rotation over an LN2 load. Six separate measurements were required to perform the polarimetric validation. Three waveplates and 3 polarizer grids at 18.7, 23.8, and 33.9 GHz were used to generate predictable Stokes brightness temperatures at the input of the FHA. The polarized grid is used to generate 3rd Stokes, and the waveplate creates 4th Stokes by essentially mixing the signals between the 3rd and 4th. Lahtinen [8]–[11] provides an excellent derivation of the Stokes parameters expected for the target as a function of grid and waveplate angle in correlation to the feed polarization. Without the waveplate, the signal produced

TABLE IV
FRONT-END PHASE BALANCE FROM PVT TEST

	18.7 GHz	23.8 GHz	33.9 GHz
Phase delta	144.5°	39.0°	-81.5°

from the target is equivalent to the signal we expect to measure during flight operation, and it allows direct application of the polarization rotation correction. An example of the test output at 18.7 GHz is given in Fig. 15 for the case of the wire grid. In this configuration, the cold and hot targets mix between the linear polarizations, and no 4th Stokes is expected. Table IV gives a summary of the front-end phase imbalance determined for each band. These angles need to be tuned on-orbit, considering the temperature range. The described procedure can be applied because the global mean of the 4th Stokes TB is zero over the ocean for all rotation angles.

With the phase balance correction in place, the antenna temperatures were computed at the feed horn input using the calibration derived from the subsystem level testing. The error computed from the measurement was <0.08 K, which is well within the allocated error.

IV. CONCLUSION

The COWVR RF subsystem testing showed that phase and amplitude were well-matched, which are required for a fully polarimetric imaging radiometer system. It was possible to measure all six Stokes parameters in the laboratory with the described polarized targets. Meeting the tight RF performance requirements was enabled by detailed planning, rigorous selection of RF components, and the matching of phase and amplitude so that two receivers worked in tandem with the RFM. The laboratory validation predicted that measurements of windspeed and vector above the sea surface are possible, which still has to be validated in orbit.

The COWVR benefitted from earlier flight developments on the Jason-3 receiver and noise source hardware and a pool of experienced engineers, including its heritage vendor MEC. The comprehensive testing of RF and dc components at the board level enabled us to meet the key requirements early in the development phase. Furthermore, mass, power, and volume were optimized without exceeding the targeted cost. The COWVR RF subsystem has surpassed most of the requirements with significant performance margins.

ACKNOWLEDGMENT

The authors would like to express gratitude to the teams involved in assembly and testing for their continuous professional support until the delivery of the COWVR RF and EU subsystems: RF assembly team (Mary Soria and Heather Lim), the DC assembly (Bradley Drake), and the RF test team (Seth Sin and Marco Chavez). This research was carried out by the Jet Propulsion Laboratory, California Institute of Technology.

REFERENCES

- [1] 2003. [Online]. Available: <http://www.nrl.navy.mil/WindSat/Description.php>
- [2] P. Gaiser *et al.*, "The WindSat spaceborne polarimetric microwave radiometer: Sensor description and early orbit performance," *IEEE Trans. Geosci. Remote Sens.*, vol. 42, no. 11, pp. 2347–2361, Nov. 2004.
- [3] F. Maiwald *et al.*, "Reliable and stable radiometers for Jason-3," *IEEE J. Sel. Topics Appl. Earth Observ. Remote Sens.*, vol. 9, no. 6, pp. 2754–2762, Apr. 2016.
- [4] 2020. [Online]. Available: <https://www.ansys.com/products/electronics/ansys-hfss-2020>
- [5] 2020. [Online]. Available: <https://www.keysight.com/it/en/products/software/pathwave-design-software/pathwave-advanced-design-system.html>
- [6] S. Brown *et al.*, "The COWVR mission: Demonstrating the capability of a new generation of small satellite weather sensors," in *Proc. IEEE Aerosp. Conf.*, 2017, pp. 1–7.
- [7] J. Zhang, P. A. R. Ade, P. Mauskopf, G. Savini, L. Moncelsi, and N. Whitehouse, "Polypropylene embedded metal mesh broadband achromatic half-wave plate for millimeter wavelengths," *Appl. Opt.*, vol. 50, no. 21, pp. 3750–3757, Jul. 20, 2011.
- [8] J. Lahtinen and M. Hallikainen, "Fabrication and characterization of large freestanding polarizer grids for millimeter waves," *Int. J. Infrared Millimeter Waves*, vol. 20, no. 1, pp. 3–20, 1999.
- [9] J. Lahtinen, A. J. Gasiewski, M. Klein, and I. S. Corbella, "Calibration method for fully polarimetric microwave radiometers," *IEEE Trans. Geosci. Remote Sens.*, vol. 41, no. 3, pp. 588–602, Mar. 2003.
- [10] J. Lahtinen and M. Hallikainen, "HUT fully polarimetric calibration standard for microwave radiometry," *IEEE Trans. Geosci. Remote Sens.*, vol. 41, no. 3, pp. 603–611, Mar. 2003.
- [11] S. H. Yueh, W. J. Wilson, F. K. Li, S. V. Nghiem, and W. B. Ricketts, "Polarimetric brightness temperatures of sea surfaces measured with aircraft K- and Ka-band radiometers," *IEEE Trans. Geosci. Remote Sens.*, vol. 35, no. 5, pp. 1177–1187, Sep. 1997.